# Effects of Rubber Content and Temperature on Unstable Fracture Behavior in ABS Materials with Different Particle Sizes

YANCHUN HAN,[2] RALF LACH,[1] WOLFGANG GRELLMANN[1]

[1] Department of Materials Science, Martin-Luther-University Halle-Wittenberg, D-06099 Halle (Saale), Germany

[2] State Key Lab of Polymer Phyics and Chemistry, Changchun Institute of Applied Chemistry, Chinese Academy of Sciences, Changchun 130022, China

*Received 8 February 1999; accepted 19 May 1999*

**ABSTRACT:** The fracture behavior of ABS materials with a particle diameter of 110 nm and of 330 nm was studied using instrumented Charpy impact tests. The effects of rubber content and temperature on fracture behavior, deformation mode, stable crack extension, plastic zone size, *J*-integral value, and crack opening displacement were investigated. In the case of a particle size of 110 nm, the material was found to break in a brittle manner, and the dominant crack mechanism was unstable crack propagation. Fracture toughness increases with increasing rubber content. In the case of a particle size of 330 nm, brittle-to-tough transition was observed. The *J*-integral value first increases with rubber content, then levels off after the rubber content is greater than 16 wt %. The *J*-integral value of a particle diameter of 330 nm was found to be much greater than that of 110 nm. The *J*-integral value of both series first increased with increasing temperature until reaching the maximum value, after which it decreased with further increasing temperature. The conclusion is that a particle diameter of 330 nm is more efficient than that of 110 nm in toughening, but for both series the effectiveness of rubber modification decreases with increasing temperatures higher than 40°C because of intrinsic craze formation in the SAN matrix at temperatures near the glass transition of SAN. © 2000 John Wiley & Sons, Inc. J Appl Polym Sci 79: 9–20, 2001

**Key words:** antibodies; instrumented Charpy impact test; *J*-integral value; plastic zone; unstable crack propagation; brittle-to-tough transition; crack opening displacement

## INTRODUCTION

As the use of polymers in structural applications increases, the fracture toughness of the polymer may become a decisive factor in material selection. Therefore, much work has been done to develop effective toughening methods for polymers. One method that has been successful in toughening brittle or notch sensitive polymers is rubber toughening.[1–3] Simply stated, rubber toughening involves the addition of elastomeric inclusions into a polymer matrix.

ABS is a family of thermoplastics that contains three monomeric units: acrylonitrile, butadiene, and styrene. Typically, a styrene acrylonitrile copolymer (SAN) matrix contains discrete butadiene-based elastomer particles for toughening.

The impact modification mechanisms for rubber-toughened polymer generally were considered to involve energy dissipation by both crazing ini-

*Correspondence to:* Y. Han.

Journal of Applied Polymer Science, Vol. 79, 9–20 (2001)

tiated from the rubber particles and cavitation of small rubber particles, which subsequently promotes localized shear deformation.[4–5] On the other hand, it is well established that crazing develops into catastrophic cracks in polymers in a single component system. Crazing is an unstable local plastic deformation together with the nucleation of voids, followed by their growth and coalescence. The brittle fracture of polymeric materials develops from the rupture of fibrils in the crazes. It was concluded that in ABS materials both deformation mechanisms, crazing and shear yield, may occur in the continuous SAN matrix.

Particle size is known to be the important parameter affecting the fracture toughness of rubber-modified materials. Sultan and McGarry[6] showed that 40 nm particles are not as efficient as 1.2 $\mu$m particles in toughening epoxies, and they therefore inferred that crazing induced by larger particles of $\sim$1 $\mu$m absorbed more energy than shear yielding induced by smaller particles of a few hundred angstroms. Kunz-Douglas et al.[7] reported that smaller particles were more effective than larger particles because the tearing energy of rubber particles increases with size decrease. Margolina and Wu[8] observed that brittle-to-tough transition occurs at the critical interparticle distance for materials toughened by shear yielding. This suggests that smaller particles are better toughening agents. Pearson and Yee[9] showed that smaller particles provide a significant increase in toughness by cavitation-induced shear bands, while large particles provide only a modest increase in fracture toughness by a particle bridging/crack deflection mechanism. According to Pearson and Yee,[9] larger particles cannot be cavitated because they lie outside the plastic zone, proposed by Irwin,[10] where large hydrostatic stress exists. Lazzeri and Bucknall[11] have proposed a model for rubber particle cavitation showing that cavitation in the rubber particles cannot be formed by particles $<0.25$ $\mu$m in diameter. Particle size cannot be adjusted independently without changing other parameters such as properties of rubber particles, volume content of rubber particles, and adhesion strength between the matrix and rubber particles.

Volume content effects were also examined by many researchers. Michler[12] claimed that maximum fracture toughness is obtained only if the average interparticle distance is between the critical minimum interparticle distance and the critical maximum interparticle distance. He explained that stress concentration is smeared over a larger volume as a consequence of the existence of entangled and interconnected macromolecules with less than the critical minimum interparticle distance, and the transition from plane strain to plane stress cannot occur with a distance greater than the critical maximum interparticle distance.

Michler[13] found that the effectiveness of particles in ABS materials for increasing toughness strongly changes depending on loading speed. In contrast to quasi-static loading conditions in a tensile test—where energy dissipation of ABS materials with 0.05 $\mu$m particles is nearly the same as that with 0.5 $\mu$m particles—under impactlike loading conditions material, with small particles it is hardly able to dissipate energy.

The influence of temperature on critical or optimum structural parameters is rarely investigated. The purpose of this article is to examine the effects of rubber content and temperature on both the mode of deformation and on the toughness of ABS materials with different particle sizes on the basis of the instability of plastic deformation.

## EXPERIMENTAL

### Materials and Samples

The materials used in this study were ABS materials with various rubber contents and two particle distributions (Figure 1 and Table I). These ABS materials were fabricated by mechanical compounding (extrusion) of various amounts of rubber particles (acrylonitrile-butadiene-styrene copolymer) made by an emulsion process[14] (and other references, cited there) with a separately produced commercial SAN ($M_w$ = 85,000 g/mol, $M_w/M_n$ = 4; proportion of styrene to acrylonitrile: 72.5:27.5; content of oligomers about 1%). After extrusion at 180°C (rubber particles were finely dispersed into a SAN matrix), specimens were formed by injection molding, in which the barrel and mold temperatures were maintained at 210°C and 70°C, respectively.

The average particle diameter, $d$, measured by ultracentrifugation, was 110 nm [small particle distribution; Fig. 1(a)] and about 330 nm [broad particle distribution; Fig. 1 (b)]. The styrene-acrylonitrile ratio in grafted SAN also formed nearly 10 nm of extended shells around the rubber particles, which was the same as in the matrix SAN.

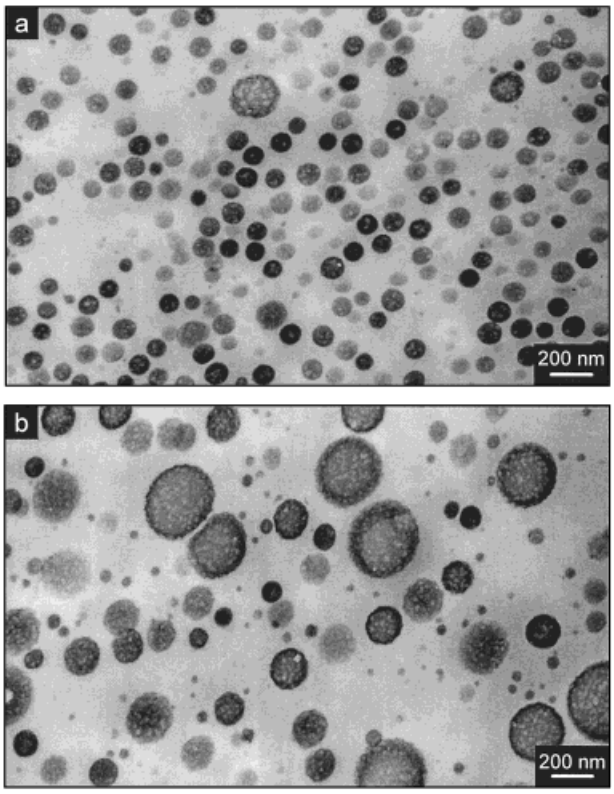


**Figure 1** Transmission electron micrographs of $OsO_4$-stained ultrathin sections of ABS materials with 16 wt % rubber: (a) $d$ = 110 nm, (b) $d$ = 330 nm.

Single-edge notched-bend (SENB) specimens were used for this study. The dimensions of the injection-molded specimen were: length, $L$ = 80 mm; width, $W$ = 10 mm; and thickness, $B$ = 4 mm. The specimens were notched with a razor blade (notch tip radius = 0.2 $\mu$m). The test conditions were optimized by simulating specimen loading using a finite element method (FEM).[15] Based on these FEM results, the experimental parameters initial crack length, $a$, = 2 mm and support span, $s$, = 40 mm were selected. The consideration of $a/W$ = 0.2 and $s/W$ = 4 enabled the determination of geometry-independent fracture mechanics values.

### Fracture Toughness Characterization

An instrumented Charpy impact tester of 4 J work capacity was used for the measurements, and measured load ($F$)–deflection ($f$) diagrams were recorded.[16] The pendulum hammer speed was set to $v_H$ = 1.0 m/s.

Impact measurements were performed to determine fracture mechanics values as resistance against unstable crack propagation. A comparison of experimentally measured and numerically computed $J$-integral values showed a distinct conformity with the results of the approximation methods of Merkle and Corten[17] and Sumpter and Turner.[18] In this study $J$-integral values were computed according to Merkle and Corten.[17] To ensure statistical safety of $J$-integral values as resistance against unstable crack propagation, at least 10 single-edge notched specimens per material were tested.

The basis of $J$-integral determination was the evaluation of measured load ($F$)–deflection ($f$) diagrams in order to calculate load, deflection, and energy quantities, such as $F_{max}$, $F_{gy}$, $f_{max}$, $f_{gy}$, $A_{el}$, and $A_{pl}$. $F_{max}$ is the maximum load and $f_{max}$ the deflection corresponding to $F_{max}$; $F_{gy}$ and $f_{gy}$ are defined at the transition point from pure elastic to elastic–plastic material behavior. $A_{el}$ and $A_{pl}$ represent the elastic and the plastic part of total deformation energy $A_g$.

Stable crack extension, $a_{BS}$, and plastic zone size were quantified on the fracture surface by light microscopy. (For those unbroken, the fracture surfaces are produced by breaking the specimens at liquid-nitrogen temperature and high pendulum hammer speed.) The effective crack length, $a_{eff}$, used for $J$-integral calculation resultws from $a_{eff} = a + a_{BS}$.

The dynamic Young's modulus, $E_d$, and the dynamic yield stress, $\sigma_{yd}$, were average values of five unnotched specimens, at $v_H$ = 1 m/s, and were calculated from pure elastic to elastic–plastic transition on the load-deflection curves of unnotched specimens according to the well-known equations of bending theory.

**Table I Designation and Composition of Investigated ABS Materials**

| | Composition $\phi_{SAN}/\phi_{ABS}$ (wt %) | |
|---|---|---|
| Material | $d$ = 110 nm | $d$ = 330 nm |
| 1 | Matrix material, SAN | |
| 2 | 96/4 | 96/4 |
| 3 | 92/8 | 92/8 |
| 4 | 88/12 | 88/12 |
| 5 | 84/16 | 84/16 |
| 6 | 80/20 | 80/20 |
| 7 | 76/24 | 76/24 |
| 8 | 72/28 | 72/28 |
| 9 | 64/36 | 64/36 |

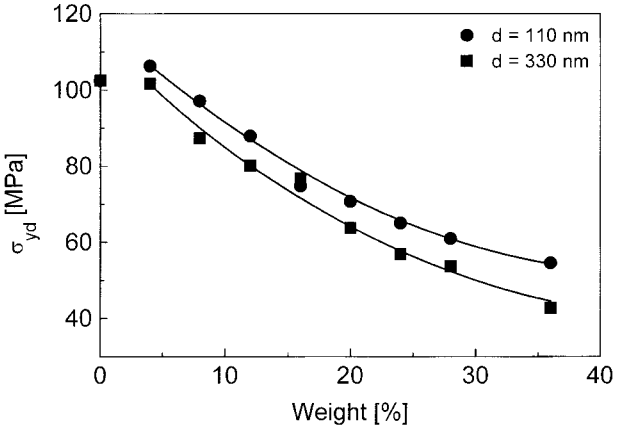


**Figure 2** Dynamic yield stress, $\delta_{yd}$, as a function of rubber content at room temperature.

The standard deviation of fracture mechanics quantities was nearly 10 % and that of both $E_d$ and $\sigma_{yd}$ was about 5 %.

## RESULTS AND DISCUSSION

### Dynamic Yield Stress and Young's Modulus

The impact behavior of untouched specimens was studied as a function of rubber content, particle size, and temperature. For all materials with particle diameters of 110 nm and 330 nm, the specimens were not broken under the test conditions.

The effect of rubber content on dynamic Young's modulus, $E_d$, and yield stress, $\sigma_{yd}$, has been investigated at room temperature. The temperature effect on $E_d$ and $\sigma_{yd}$ has also been studied for rubber content of 4 wt %, 16 wt %, and 28 wt % for both series.

$\sigma_{yd}$, as a function of rubber content and temperature [demonstrated in Figs. 2 and 3(a,b), respectively], decreases with increasing rubber content and temperature, and the $\sigma_{yd}$, of those with a particle diameter of 110 nm is larger than those with a rubber particle diameter of 330 nm. This means that a higher rubber content and a larger rubber particle size reduce the strength of the composite because one of the functions of the rubber domains is to create stress concentrations, forcing the material to yield at lower applied stresses.

The rubber content effect on dynamic Young's modulus, $E_d$, is illustrated in Figure 4 as well as the temperature effect on $E_d$, shown in Figure 5(a,b), for both series with rubber content of 4 wt %, 16 wt %, and 28 wt %, respectively. As shown in these figures, $E_d$ tends to decrease with increasing rubber content and temperature. It is known that higher rubber content and larger rubber particle size reduce the stiffness of the composite.

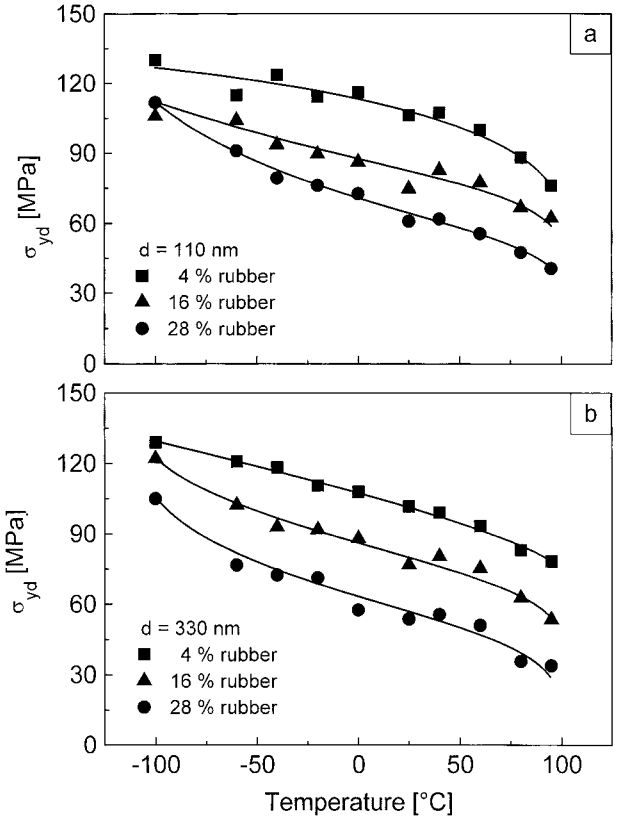


**Figure 3** Dynamic yield stress, $\delta_{yd}$, as a function of temperature: (a) $d$ = 110 nm, (b) $d$ = 330 nm.

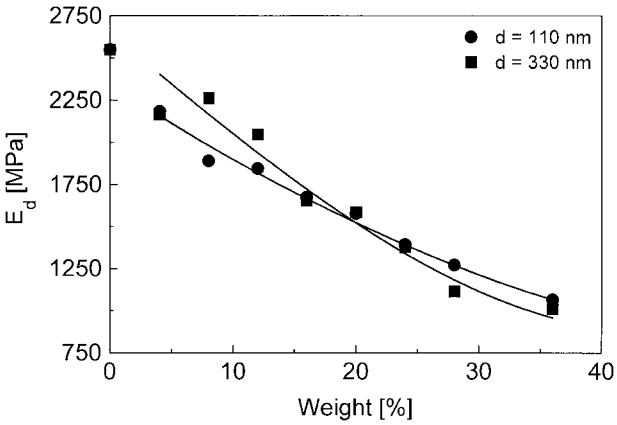


**Figure 4** Young's modulus, $E_d$, as a function of rubber content at room temperature.

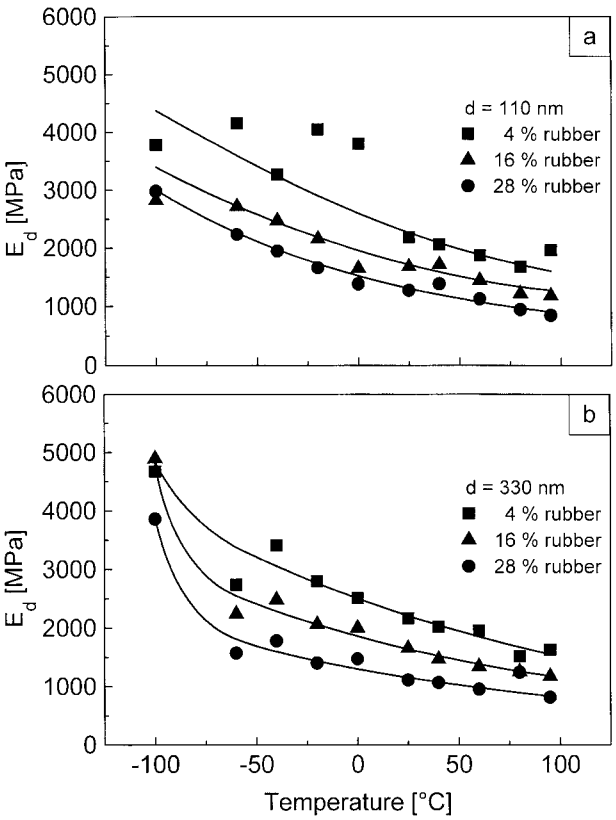


**Figure 5** Young's modulus, $E_d$, as a function of temperature: (a) $d$ = 110 nm, (b) $d$ = 330 nm.

### Load-Deflection Diagrams of Notched Specimens

Figure 6 shows typical load ($F$)–deflection ($f$) diagrams of ABS materials obtained under different test conditions. It can be seen from Figure 6(a) that the material possesses a linear load-deflection curve up to a maximum, followed by unstable crack propagation, which is indicated by the nearly vertical drop in the load-deflection curve. It is expected that fractures are either brittle or semibrittle in nature. The main deformation process is elastic deformation, and the dominant crack growth mechanism is unstable crack propagation. In Figure 6(b) the material presents elastic–plastic fracture behavior, but the dominant crack growth mechanism is still unstable crack propagation. Only $F$–$f$ diagrams, as shown in Figure 6(a,b), can be observed for materials with a particle size of 110 nm. The diagram in Figure 6(c) shows elastic–plastic fracture behavior, and the crack growth is both unstable and stable crack propagation. However, in Figure 6(d) the material is elastic–plastic with stable crack propagation. For those with a particle size of 330 nm, all the cases in Figure 6 can be seen under different test conditions.

The diagrams in Figure 6 show three transitions of mechanical behavior. The first transition occurs from pure elastic to elastic–plastic material behavior with predominantly unstable crack growth. In these regions the specimens break in a brittle manner. The second transition is from unstable crack propagation to unstable and stable crack propagation. The third transition to predominantly stable crack growth without sample fracture is characterized by means of the large crack propagation energies, $A_R$. The decreasing deflection values at the end of the experiment are caused by rebound of the pendulum striker from the sample. Therefore, the third transition can be designated a brittle-to-tough transition.

From the load-deflection behavior it may be deduced that a uniform toughness characterization of these materials, depending on concentration, is not possible if one considers previous knowledge of the use of different fracture mechanics concepts. The toughness characterization of those with a rubber particle diameter of 110 nm and those with a rubber particle diameter of 330 nm at the lower rubber content must be carried out with fracture mechanics values that characterize materials resistance to unstable crack growth because of the dominant unstable crack growth mechanism (for instance $J$-integral, the evaluation method of Merkle and Corten[17]). The toughness characterization of those with a rubber particle diameter of 330 nm and with a higher rubber content must be accomplished using crack resistance ($R$) curves.

### Stable Crack Propagation and Plastic Zone

Even though the dominant crack mechanism is unstable, fracture surface analysis shows that stable crack propagation still occurs in materials with particle diameters of 110 nm and 330 nm with lower rubber content (less than 16 wt %). The schematic diagram showing formation of various zones ahead of the crack tip is illustrated in Figure 7. On the fracture surface, (1) represents the initial notch, (2) is the stable fracture surface where shear deformation occurs, and (3) is the damaged area where craze was produced. The craze zone and zone of shear deformation consist of the plastic zone. Representing the unstable fracture surfaces if the material breaks in a brittle manner is (4). For a ductile fracture it represents an undamaged area.

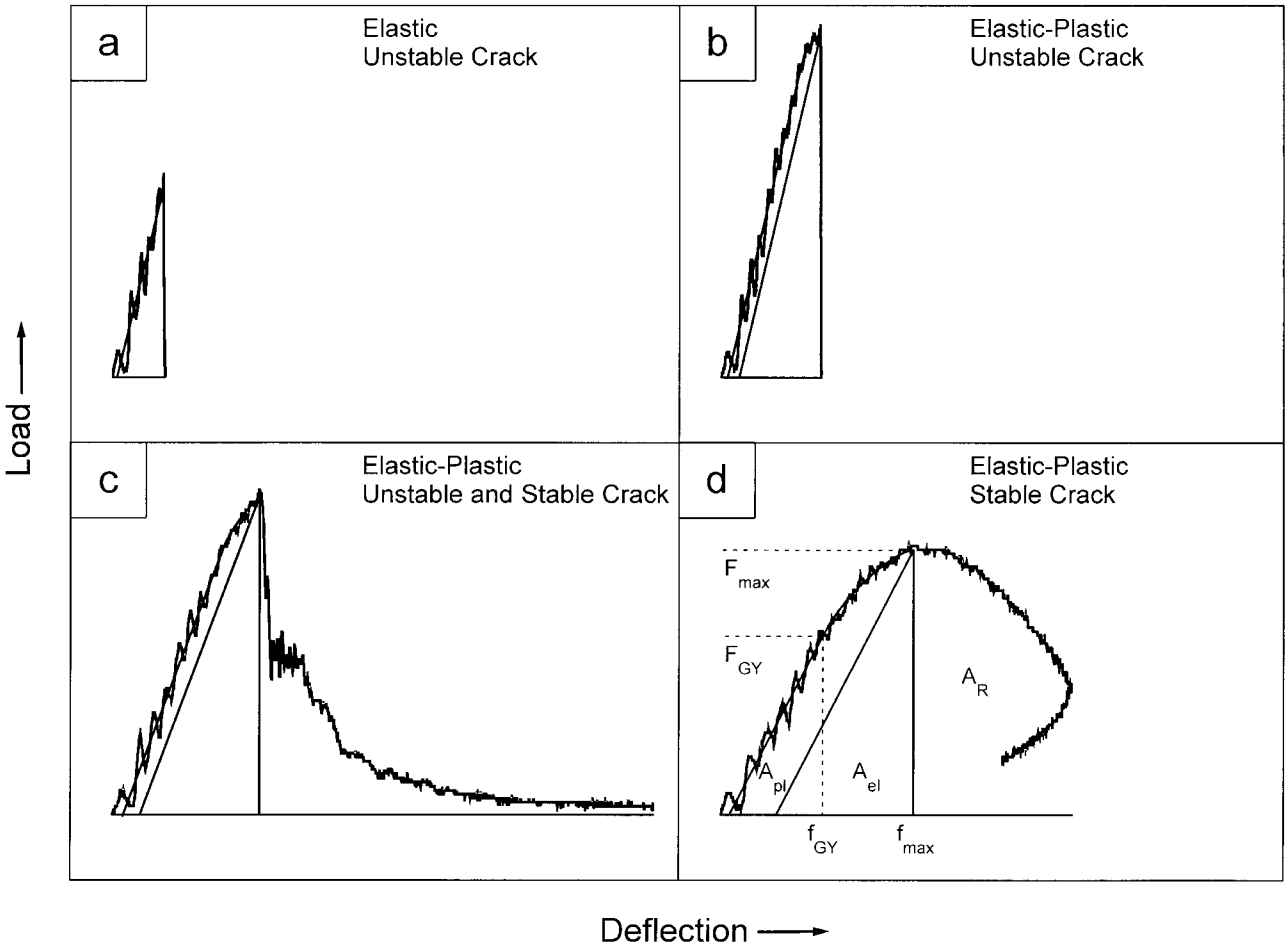


**Figure 6** Typical load ($F$)–deflection ($f$) curves of ABS materials recorded during instrumented impact tests

Optical micrographs show, especially for 330 nm ABS with 16 wt % rubber at temperatures higher than room temperature, a fracture surface more modified than that illustrated in Figure 7. In this case, (4) represents another stable fracture surface corresponding to crack propagation energy, $A_R$, (Figure 6), where stress whitening of the fracture surface shows a maximum at room temperature and is not so intensive at higher as well as at lower temperatures.

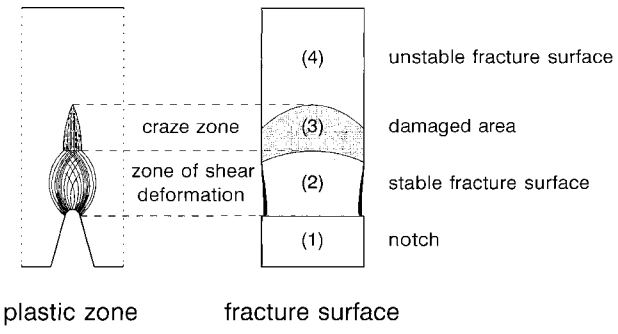


**Figure 7** Schematic diagram showing formation of various zones ahead of the crack tip.

By means of *in situ* techniques using a high-voltage electron microscope it can be found that thin ABS samples (ABS with an average particle diameter of 270 nm and a rubber content of 16 wt % is comparable to the 330 nm ABS investigated in this study) show highly plastic deformation by shear flow corresponding to formation of holes inside of rubber particles.[19] Because of the observed kinetics of the fracture process for (1) the formation of a plastic zone corresponding to the blunting of the sharp notch; (2) a stable crack initiation and propagation, which can be corresponded to stable crack extension, $a_{BS}$; and (3) an unstable crack propagation, bulk material for 330

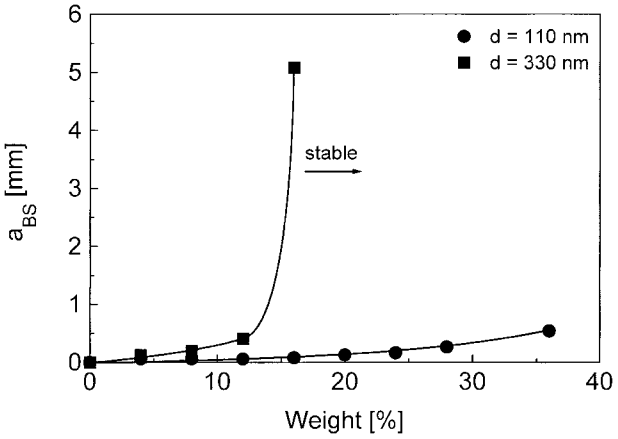


**Figure 8** Stable crack extension, $a_{BS}$, as a function of rubber content at room temperature.

nm ABS should also show this micromechanical deformation mechanism as the most dominant. However, from typical fracture surface phenomena [area (3) in Fig. 7] formation of crazes can be concluded for 110 nm material as well as for 330 nm material at lower rubber weights and/or lower temperatures.

Figure 8 shows the rubber-content effect on the stable crack extension, $a_{BS}$, for rubber particle diameters of 110 nm and 330 nm. In the case of 110 nm, the stable crack extension is very small and increases with increasing rubber content. But in the case of 330 nm, when the rubber content is less than 16 wt %, the stable crack extension increases with increasing rubber content. When the rubber content is greater than 16 wt %, the crack mechanism is only stable crack propagation—the stable crack propagation is not followed by break of specimens because the energy of the pendulum hammer is not high enough.

The temperature effect on the stable crack extension is also investigated for rubber content of 4 wt %, 16 wt %, and 28 wt % with particle diameters of 110 nm and 330 nm, shown respectively in Figure 9(a,b). For a particle diameter of 110 nm ABS materials, the stable crack extension, $a_{BS}$, tends to increase with increasing temperature until reaching the maximum value. After that, it decreases with further increasing temperature. For those with a rubber particle diameter of 330 nm, when the rubber content is 4 wt %, the stable crack extension changes very slowly with increasing temperature, and the fracture behavior is always brittle at any temperature. But for those with rubber content of 16 wt % and 28 wt %, the changes are obvious. For a rubber content of 16 wt %, the stable crack extension reaches the maximum at a temperature of 20°C. That means the fracture behavior at 20°C is more stable than at temperatures lower or higher than 20°C. And for a rubber content of 28 wt %, after increasing $a_{BS}$ at temperatures up to −40°C, only stable crack propagation and no break of specimens can be found.

The plastic deformation mechanisms, which are also the toughening mechanisms in ABS, are basically crazing, cavitation, and shearing. The study of the plastic zone size in ABS may help explain how the rubber particles contribute to plastic deformation and fracture toughness.

As a load is applied to the specimen, the local plastic zone initiates from the tip of the notch. A maximum stress then develops at the tip of the local plastic zone that spreads across the ligament thickness ahead of the notch under the plane strain, which is distinct from the stress distribution ahead of the notch under the elastic state. When the stress ahead of the plastic zone reaches a critical stress by the extension of the

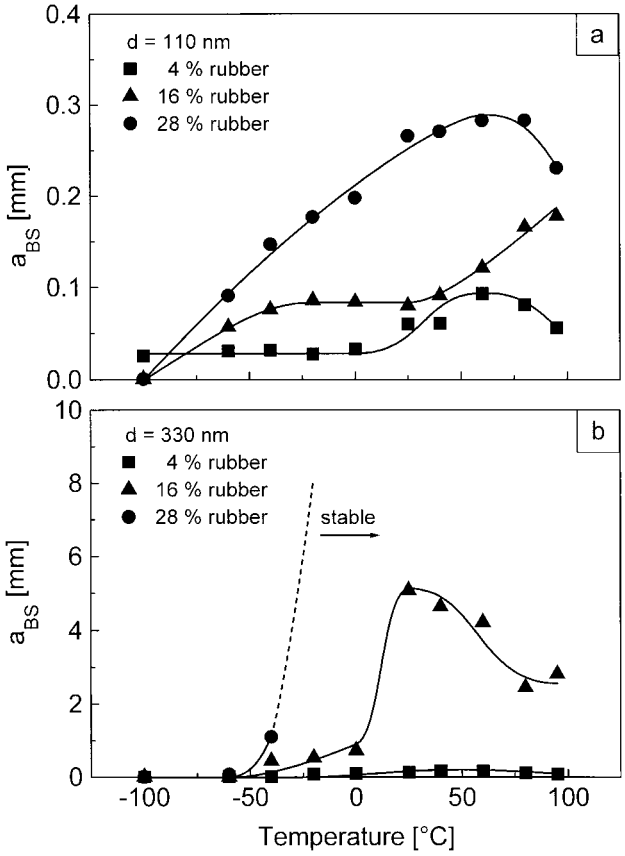


**Figure 9** Stable crack extension, $a_{BS}$, as a function of temperature: (a) $d$ = 110 nm, (b) $d$ = 330 nm.

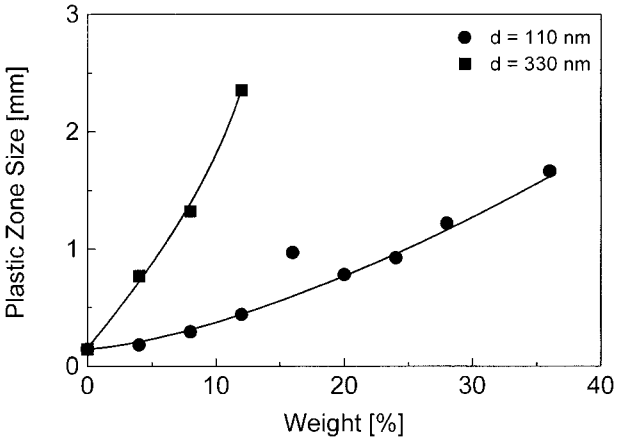


**Figure 10** Plastic zone size as a function of rubber content at room temperature.

plastic zone, the development of the internal craze, in which the plastic strain is locally concentrated between neighboring voids, occurs at the tip of the local plastic zone. If the stress ahead of the local plastic zone reaches the level of the strength of the fibrils of the craze, then microrupture of the fibrils of the craze leads to catastrophic brittle fracture.

Plastic zone size as a function of rubber content of two ABS series is illustrated in Figure 10. Plastic zone size increases with increasing rubber content. The plastic zone size of the materials with 330 nm is greater than that for the corresponding material with 110 nm. In the case of 330 nm, when the rubber content is greater than 16 wt %, the crack becomes stable.

Figure 11 (a,b) demonstrates the temperature effect on plastic zone size for rubber particle diameters of 110 nm and 330 nm with a rubber content of 4 wt %, 16 wt %, and 28 wt %. For those with a rubber diameter of 110 nm, plastic zone size increases with increasing temperature until it reaches the maximum value. After that, it decreases with any further temperature increase.

For those with a rubber particle diameter of 330 nm when the rubber content is 4 wt %, the crack propagation mechanism is still unstable crack. Plastic zone size increases with temperature until the temperature is 40°C; after that plastic zone size decreases with increasing temperature. For a rubber content of 16 wt %, the crack propagation becomes predominantly stable when the temperature is higher than 0°C. For a rubber content of 28 wt %, the crack propagation becomes stable when the temperature reaches −20°C. For the unstable crack propagation, plastic zone size increases with increasing temperature for both rubber content.

Assuming a qualitative correlation between stable crack extension and plastic zone size, respectively, and energy dissipation with respect to the kind of deformation (craze formation, shear yielding, etc.), plastic zone size as a quantity of deformation capacity also gives information about energy dissipation, reflected for example in $J$-integral values.

Crack stability can be reduced during measurements by physical aging, especially at higher temperatures. However, before heating specimens to make temperature-dependent fracture mechanics experiments, it is necessary to level out differences between specimen temperature and external temperature. Experimental practice shows that for a temperature difference lower than 2 K, a half hour is required. This time is too short to produce significant physical aging for temperatures lower than 10 K below the glass temperature of the SAN matrix, $T_g$ ($T_g$ = 108°C, measured using differential scanning calorimetry). That is why an increase of $a_{BS}$ and plastic

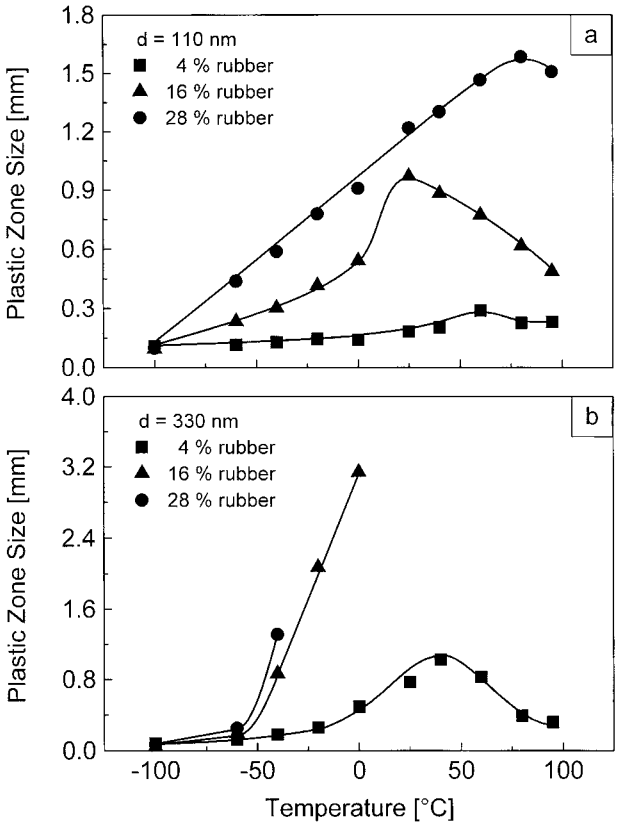


**Figure 11** Plastic zone size as a function of temperature: (a) $d$ = 110 nm, (b) $d$ = 330 nm.

zone size, shown in Figures 9 and 11, is not an effect of physical aging but is caused by characteristics of the SAN matrix.

In contrast to conventional extrinsic crazes initiated at regions of stress concentration (for example, at small surface cracks and at holes or particles, etc., inside the material), intrinsic crazes are formed inside the material, where any dependence on structural heterogeneities cannot be found. The initiation and growth of intrinsic crazes at temperatures near the glass transition is typical for such amorphous polymers as PC, PVC, and SAN.[13,20,21] As an example, for PC, intrinsic crazes are found above temperatures of 15 K to 20 K lower than $T_g$ at (quasi)static loading conditions (corresponding to external deformation speeds in the order of mm/min and lower.[13] Because of the stress-induced increase of Tg,[22,23] to describe initiation of crazes theoretically,[13,22] it can be assumed that intrinsic crazes are already growing under impactlike loading conditions at much lower temperatures (for example, room temperature).

In summary it may be said that effectiveness of rubber modification decreases with increasing temperatures, which can be also observed in this study. This "embrittlement" at higher temperatures is comparatively more important than conventional brittle-to-tough transition at lower temperatures because of its influence on applications of normally ductile polymeric materials at higher temperatures (for example, surface temperatures of polymer components by radiation with sunlight in summertime can reach 80°C and more).

In the future it will be necessary to clearly detail temperature dependencies on morphological parameters (for example, averaged particle diameter and averaged interparticle distance) in correlation with micromechanical deformation mechanisms. In this connection a key question is: Are, as Wu[1,8,24] assumes, optimum particle size and critical interparticle distancereally material characteristics for a given matrix material?

### *J*-Integral Value

The application of the *J*-integral concept enables an energetic interpretation of the failure behavior of materials. The calculation of the *J*-integral includes the analysis of load-determined and deformation-determined parameters. The *J*-integral values of two ABS series as a function of rubber content are shown in Figure 12. For the material with particle diameter of 110 nm as well as of 330 nm, the *J*-integral value increases with increasing rubber content and reaches a maximum level (the high-level toughness) when the rubber content is greater than 16 wt %. From Figure 12 it can be seen that with increasing rubber content the *J*-integral of 330 nm is much greater than that of 110 nm.

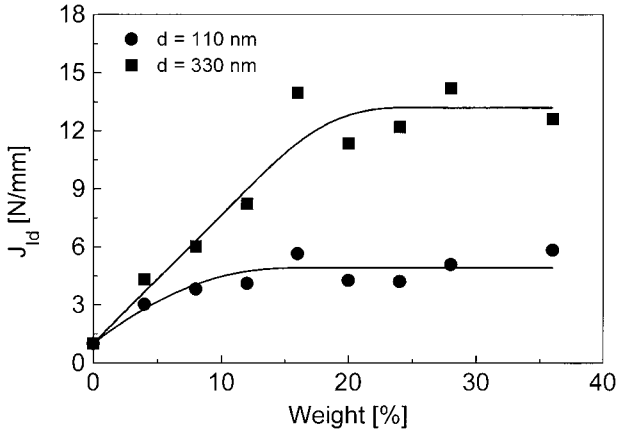


**Figure 12** *J*-integral values against unstable crack propagation, $J_{Id}$, as a function of rubber content at room temperature.

Figure 13(a,b) illustrates the temperature effect on the *J*-integral value for rubber particles with a diameter of 110 nm and 330 nm and rubber contents of 4 wt %, 16 wt %, and 28 wt %. A *J*-integral value increases with increasing temperature until it reaches the maximum value; after that, a *J*-integral value decreases with further increasing temperature. Two reasons cause the decreasing *J*-integral value at a high temperature: the reduction of the Young's modulus at high temperature and the embrittlement of the SAN matrix at temperatures relatively close to its glass transition, which is discussed in the section "Stable Crack Propagation and Plastic Zone."

The effect of particle size is evident. Small, 110 nm diameter particles are not as efficient in providing a toughening effect as large, 330 nm diameter particles, which appear to be the most efficient and provide more than a 10-fold increase in fracture toughness. With a particle diameter of 110 nm, although the rubber increases the toughness of the brittle SAN matrix by a factor of 3–6, the blends are still brittle. Thus, the rubber only increases the toughness of the brittle matrix without making the blends tough. With a particle diameter of 330 nm, the rubber not only increases the toughness of brittle SAN matrix but also make it tough when rubber content is greater than 16 wt %.

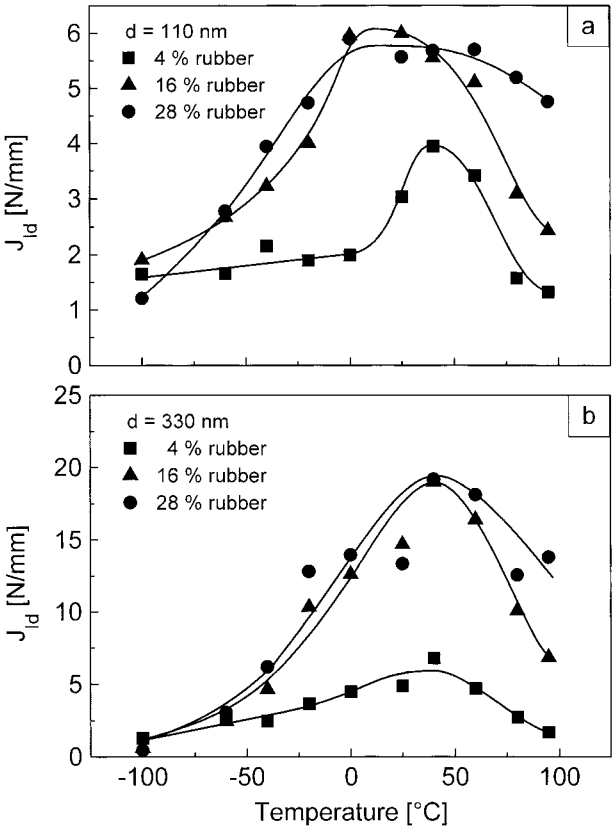


**Figure 13** *J*-integral values against unstable crack propagation, $J_{Id}$, as a function of temperature: (a) $d$ = 110 nm, (b) $d$ = 330 nm.

Based on the results of a this and other recent studies,[25] brittle-to-tough transition (BTT) rubber weights are determined by averaging low- and high-level toughness. In principle, two kinds of fracture mechanics values can be used to estimate BTTs: First, crack toughness values, $J_{0.2}$, as resistance against stable crack initiation calculated by evaluation of crack resistance curves at a stable extension of 0.2 mm (engineering initiation values); and second, crack toughness values, $J_{Id}$, as resistance against unstable crack initiation.[26] In contrast to BTT rubber weights as resistance against stable crack initiation, which are nearly independent on temperature, BTT rubber weights as resistance against unstable crack initiation show pronounced steps from low-level to high-level values at temperature ranges of 80–95°C ($d$ = 330 nm; Fig. 14). From that we believe there's a significant change in the micromechanical process at increasing temperatures. Because unstable crack propagation is normally initiated by stable crack propagation, so BTT rubber weights defined as resistance against unstable crack initiation are smaller or nearly equal than resistance against stable crack initiation.

## Crack Opening Displacement

The critical crack opening displacement is determined by the instrumented Charpy impact test based on the plastic hinge model[27]

$$\delta_{Id} = \frac{1}{n}(W - a)\frac{4f_{max}}{S}$$

where $n$ is the rotational factor ($n$ = 4).

For polymeric materials with large plastic deformation, only processes in the crack tip should be considered in calculating the critical crack opening displacement. This is because differences between the actual crack opening displacement and that calculated from $f_{max}$ will increase with increasing plastic deformation. This critical value is denoted as $\delta_{Idk}$. To determine $\delta_{Idk}$, it is necessary to substitute the maximum deflection, $f_{max}$, by the notch contribution of deflection, $f_k$. The notch contribution, $f_k$, is calculated by $f_k = f_{max} - f_b$, where $f_b$ is the deflection of the unnotched part of specimen, computed using bending theory.[28,29]

The crack opening displacement, $\delta_{Idk}$, as a function of rubber content, is demonstrated in Figure 15. The $\delta_{Idk}$ increases with increasing rubber content for both particle diameters, 110 nm and 330 nm, without reaching a clear maximum level at a

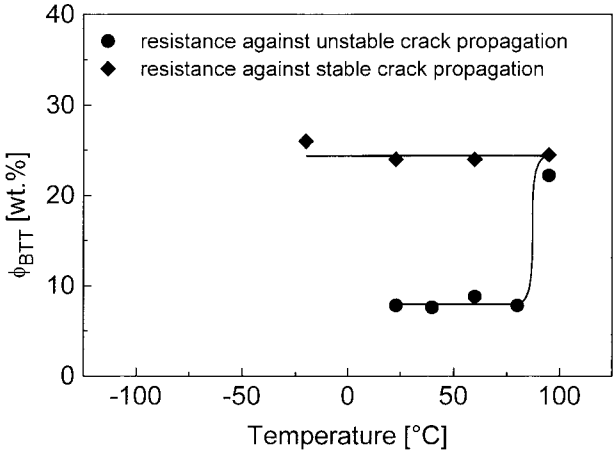


**Figure 14** Brittle-to-tough transition (BTT) rubber weights, $\phi_{BTT}$, as a function of temperature ($d$ = 330 nm); data from this and other studies[25] (spheres: BTT rubber weights as resistance against unstable crack propagation; diamonds: BTT rubber weights as resistance against stable crack propagation).

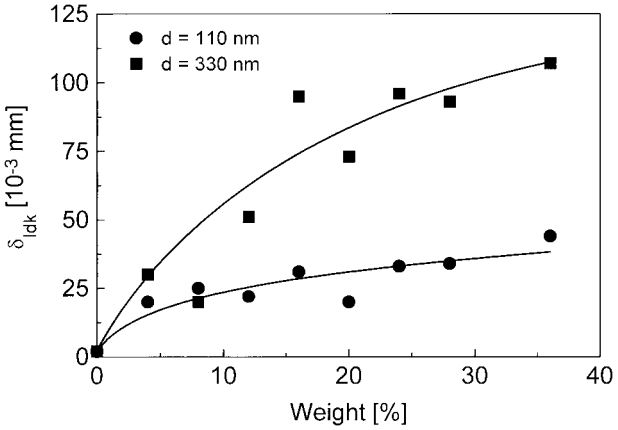


**Figure 15** Crack opening displacement, $\delta_{Idk}$, as a function of rubber content at room temperature.

higher rubber content, in contrast to the *J*-integral value. The $\delta_{Idk}$ of the particle diameter of 330 nm is greater than that of 110 nm, especially when the rubber content is greater than 12 wt %.

The effect of temperature on the crack opening displacement for both series was also investigated. The result is illustrated in Figure 16(a,b). It can be seen that the variation of crack opening displacement with temperature has the same trend as the variation of *J*-integral with temperature: Before reaching a certain temperature, the crack opening displacement increases with increasing temperature. After that it decreases with further increasing temperature.

However, it must be pointed out that for ABS, the maximum point corresponding to *J*-integral is not the same as that corresponding to $\delta_{Idk}$, which is exemplified by the temperature dependencies of both *J*-integral and $\delta_{Idk}$ for 110-nm ABS material with 4 wt % rubber. The observed temperature difference of about 40 K indicates that it is necessary to use a multiparametric description method to consider the different influences of load and deflection on the fracture process. Comparable results were obtained for brittle-to-tough transition (BTT) temperatures, estimated by averaging low- and high-level toughnesses.[19] At rubber weights higher than 24 wt % BTT, temperatures corresponding to *J*-integral and $\delta_{Idk}$ differ from each other.

From all the above results, it be clearly seen that the larger particle size (diameter of 330 nm) is more effective in toughening than the smaller particle size (diameter of 110 nm). Increasing rubber content can also increase the toughening effect. The improvement in toughness with an increase in rubber volume content has been attributed largely to the increase in the number of craze initiation sites and to the change from predominant craze formation to predominant shear flow. Temperature has a different effect on the fracture toughness: ABS materials displayed a peak fracture toughness at about 40°C, but the toughness decreased for both lower and higher temperatures. The decrease in toughness with temperature may be explained in terms of competition between the critical opening displacement (COD) and the yield stress. If the decrease in yield stress outweighs the increase in COD, the fracture toughness is reduced as temperature is increased.

## CONCLUSIONS

1. Fracture toughness (*J*-integral values and COD values) for 110-nm and 330-nm ABS materials increases with increasing temperature until reaching a maximum value, after which it decreases with additional in-

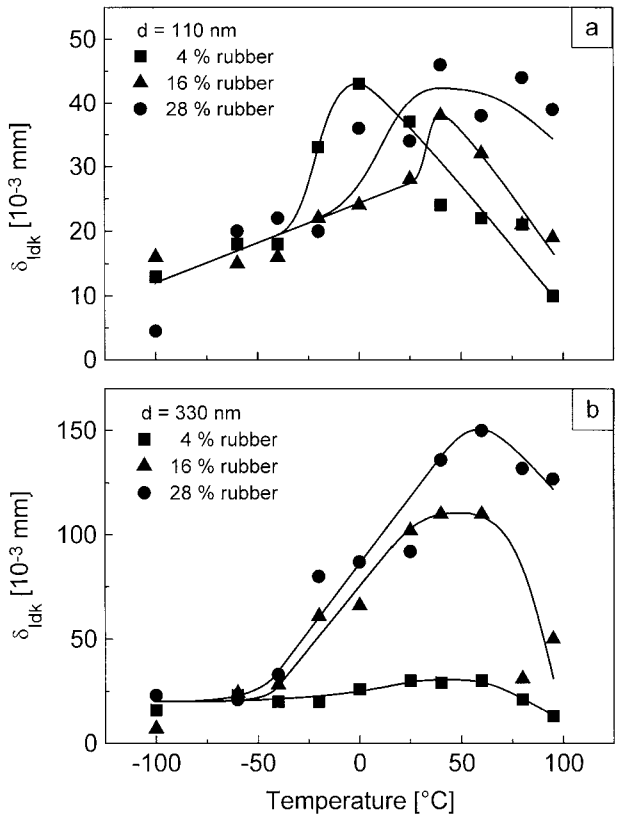


**Figure 16** Crack opening displacement, $\delta_{Idk}$, as a function of temperature: (a) $d$ = 110 nm, (b) $d$ =330 nm.

creasing temperature (but rubber modification of 330-nm ABS is much more effective than that of 110-nm ABS). This is because of the reduction in Young's modulus at a higher temperature and the intrinsic craze formation in the SAN matrix at temperatures close to the glass transition of SAN. This matrix "embrittlement," which reduces the effectiveness of rubber modification significantly, can be discussed in terms of the temperature dependencies of stable crack extension and plastic zone size because there are qualitative correlations between fracture surface phenomena and energy dissipation processes.

2. Brittle-to-tough transition (BTT) rubber weights as resistance against unstable crack propagation show pronounced steps from low- to high-level values because of the effect of matrix embrittlement. Because stable crack propagation is normally sequential to unstable propagation, BTT rubber weights, as resistance against unstable crack propagation, are nearly equal or smaller than that as resistance against stable crack propagation, in which the latter are independent of temperature.
3. From temperature differences of maximum $J$-integral and COD values, as a consequence of the different influences of load and deflection on toughness behavior, it can be concluded that it is necessary to use a multiparametric description of the fracture process.

The authors gratefully acknowledge Bayer AG, Leverkusen and especially Dr. P. Krüger for making the ABS materials available. In addition, the authors wish to thank Dr. P. Krüger making available TEM micrographs and particle size determination by ultracentrifugation. Y. C. Han wishes to thank DAAD-K. C. Wong Foundation for her research fellowship at Martin-Luther-University Halle-Wittenberg. The authors also acknowledge financial support from Deutsche Forschungsgemeinschaft (DFG).

## REFERENCES

1. Wu, S. Polymer 1985, 26, 1855.
2. Bucknall, C. B. Toughened Plastics; Applied Science: London, 1977.
3. Parker, D. S.; Sue, H.-J.; Huang, J.; Yee, A. F. Polymer 1990, 31, 2267.
4. Donald, A. M.; Kramer, E. J. J Appl Polym Sci 1982, 28, 3719.
5. Kinloch, A. J.; Young, R. J. Fracture Behavior of Polymers; Applied Science: London, 1983.
6. Sultan, J. N.; McGarry, F. J. Polym Eng Sci 1973, 13, 29.
7. Kunz-Douglas, S. C.; Beaumont, P. W. R.; Ashby, M. F. J Mater Sci 1980, 15, 1109.
8. Margolina, A.; Wu, S. Polymer 1988, 29, 2170.
9. Pearson, R. A.; Yee, A. F. J Mater Sci 1991, 26, 3828.
10. Irwin, G. R. Appl Mater Res 1964, 3, 65.
11. Lazzeri, A.; Bucknall, C. B. J Mater Sci 1993, 28, 6799.
12. Michler, G. H. Acta Polymerica 1993, 44, 113.
13. Michler, G. H. Kunststoff–Mikromechanik–Morphologie, Deformations– und Bruchverhalten; Hanser: München, Wien, 1992.
14. Eichenbauer, H.; Ott, K.-H. In Acrylonitrile–Butadiene–Styrene (ABS) Polymers; Evers, B., Ullmann, F., Eds.; Ullmann's Encyclopedia of Industrial Chemistry; VCH: Weinheim, 1992; Vol. A21, Chapter 5, p 633.
15. Grellmann, W.; Sommer, J. P. Fracture Mechanics and Coupled Fields; FMC Series: Chemnitz, 1985; Vol. 17, p 48.
16. Grellmann, W.; Seidler, S.; Hesse, W. In Deformation and Fracture Behavior of Polymers; Grellmann, W.; Seidler, S., Eds.; Springer: New York, Berlin, Heidelberg, to be published.
17. Merkle, J. G.; Corten, H. T. J Pressure Vessel Technol 1974, 6, 286.
18. Sumpter, J. D. G.; Turner, C. E.; ASTM STP 1976, 601, 3.
19. Lach, R.; Grellmann, W.; Krüger, P. In Deformation and Fracture Behavior of Polymers; Grellmann, W.; Seidler, S., Eds.; Springer: New York, Berlin, Heidelberg, to be published.
20. Dettenmaier, M.; Kausch, H. H. Polymer 1983, 21, 1232.
21. Dettenmaier, M. In Crazing in Polymers; Kausch, H. H.; Ed.; Springer: Berlin, Heidelberg, 1983; p 57.
22. Starke, J.-U.; Schulze, G.; Michler, G. H. Acta Polymerica 1997, 48, 92.
23. Lach, R.; Grellmann, W.; Schröter, K.; Donth, E. Polymer 1999, 40, 1481.
24. Wu, S. Polym Mater Sci Eng 1990, 63, 220.
25. Han, Y.; Lach, R.; Grellmann, W. J Appl Polym Sci, to appear.
26. Grellmann, W.; Seidler, S.; Jung, K.; Kotter, I. J Appl Polym Sci, to appear.
27. Kobayashi, T. Eng Fracture Mechanics 1984, 16, 67.
28. Hoffmann, H.; Grellmann, W.; Zilvar, V. In Proceedings of the 28th Microsymposium on Macromolecules Polymer Composites; Walter de Gruyter & Co.: Berlin and New York, 1986; p 233.
29. Grellmann, W.; Jungbluth, M. Fracture Mechanics and Coupled Fields; FMC Series; Chemnitz, 1987; Vol. 37, p 186.